Radial roller bearings with flexible rings: application to rotor dynamics and extension to multibody simulations

Mikhail Leontiev[1], Vladimir Ivannikov[2]*, Sergey Degtyarev[2]

ISROMAC 2017

International Symposium on Transport Phenomena and Dynamics of Rotating Machinery

Maui, Hawaii

December 16-21, 2017

Abstract

To obtain reliable assessments of the roller bearing durability the credible values of the radial forces are required. Most of the existing bearing models omit structural deformations of rings. This assumption does not hold for modern jet engines, where shafts are commonly hollow and the housing and the rings thicknesses may be of comparable magnitudes. Furthermore, if a considerable negative internal clearance occurs at the bearing at its operating regime and the bearing rings are said to be rigid, the computed radial contact forces may be significantly overestimated. To account for this phenomenon, a simplified deformation pattern of a ring is considered, which implies its discretization into finite segments subjected to constant tensile/compressive forces and constant bending moment. The model key relations are derived from the energy functional that describes equilibrium of a roller located between two rings. The obtained expressions are used to build a specific 2-nodes bearing finite element, which can be conveniently applied for rotor dynamics problems. A numerical example is used to demonstrate workability and performance of the approach. The results are verified using 3D NX Nastran FE model.

Keywords

radial roller bearing — flexible rings — rotor dynamics — jet engines — structural deformations

[1] *Moscow Aviation Institute, Moscow, Russia*

[2] *Alfa-Tranzit Co. Ltd, Moscow, Russia*

*__Corresponding author__: vladimir@civil.ist.utl.pt

1. INTRODUCTION

The problem of the internal bearing forces analysis has been well studied in the past 50 years, since their accurate determination is an important departure point for credible subsequent durability assessment. Since the complete solution of this problem involves various physical phenomena, *i.e.*, elastic deformations, contact interactions, inertia effects, elastohydrodynamics, a large range of mathematical models, which reproduce one or the other aspects of the bearing behavior. The simplest analytical approaches were gathered and well described by Palmgren [18]. The detailed analysis of the ball bearing equilibrium with centrifugal forces was performed by Harris [11]. Liu [15] prepared similar formulation of the tapered roller bearing model. A unified formulation for determination of equilibrium in both ball and roller bearings was presented by Mul et al. [16, 17]. Aihara [1] estimated the friction forces and the flanges contributions to the distribution of the bearing internal forces. This model was further advanced in the work of Aramaki et al. [3], where the inertia and contact effects arising from the bearing separator were additionally considered. Besides that the authors accounted for the rings expansion due to their rotation. The influence of all the discussed factors was summarized by Gupta [10].

However, in the aforementioned contributions the bearing rings were said to be rigid. It is worth noting that the effect of the bearing rings structural deformations remains one of the least studied factors influencing the distribution of the bearing radial forces. This contribution is particularly important for supports whose rings are flexible. The bearings of this type are commonly used in modern jet engines, where shafts are commonly hollow and the housing and the outer ring thicknesses may be of comparable magnitudes. If a considerable negative internal clearance occurs at the bearing at its operating regime, the computed radial forces may be significantly overestimated.

In general case the deformed state of the bearing rings is difficult to determine and a spatial finite element problem with large number of degrees of freedom has to be solved to this end. To handle it correctly, besides the accurate modeling of contact between the roller and the rings, one needs to pay special attention to the kinematic constraints to be enforced onto the latter. Imposition of the kinematic boundary conditions directly onto rings surfaces commonly reveals problematic and in order to circumvent this issue, the rotor components neighbouring to the bearing, with easier to define kinematic restraints, are added to the three dimensional assembly. Such approach is safer and less prone to modeling errors and allows one to expect results of higher quality, but it is computationally expensive and nearly unacceptable for rotor dynamics problems of gas turbine engines with several antifriction bearings.

Among the developed simplified bearing models very few of them account for the bearing flexibility. One of the first attempts to build such a model was made by Jones and

Harris [13], who incorporated the outer ring deformations into the bearing model, although for a very particular case — the support of an idler gear in a planetary transmission. Later Filetti and Rumbarger [7], developing a general method for predicting the influence of structural support upon bearing performance, handled the outer ring as a set of beam elements and used 1D linear springs for the rollers in contact. The assembly of the ring and the rollers itself had two connection nodes with the ground support. This model proved to have good correlation with experimental data, however, the a priori knowledge about the attachment points of the outer ring significantly limits the approach applicability. Moreover, likewise the formulation of Jones and Harris [13], in the model of Filetti and Rumbarger [7] only one of the bearing rings is deformable. Cheng [6] advanced this approach and included in the finite element assembly not only the outer ring itself, but also the neighbouring regions of the housing.

Perhaps, one of the first simplified bearing models which accounted the deformations of both rings was presented by Cavallaro et al. [5], further extended by Leblanc et al. [14]. Distinctly from previous formulations, the problem of determination of the rings deformations was formulated in terms of forces. The model also considered the centrifugal expansion of the rings, the cage rotation and the lubricant presence. The ring out-of-roundness produced by a single line contact load was expressed through a Fourier series and the effects of these contributions were superimposed afterwards to draw the resultant deformed shape of the ring. The Newton–Raphson method is then used to simultaneously solve the equilibrium and geometric equations. The corresponding flexibility matrix constructed on the basis of the Fourier series term turns out ill-conditioned thus affecting the iterative procedure stability, especially, when a roller enters or leaves the contact zone.

In the present contribution to incorporate structural flexibility the simplified deformation pattern of the bearing rings is introduced. This implies the ring discretization into finite segments subjected to constant tensile/compressive forces and constant bending moment. The centrifugal load acting on the roller is also considered. To derive the roller equilibrium equations and the subsequent bearing resultant force vector with the corresponding tangent stiffness matrix the minimization of the total energy functional, constructed for each roller separately, was invoked. Besides the radial deflections of the rings, the formulation also permits their misalignments. The model workability is demonstrated in numerical examples.

2. RADIAL BEARING MODEL

2.1 Bearing equilibrium

Consider a bearing as an element with two nodes A and B, attached to centers of inner and outer rings, respectively, see Figure 1. We introduce a cartesian system x, y, z, whose origin coincides with node A. Its unitary vectors are $\mathbf{e}_{x0}$, $\mathbf{e}_{y0}$, $\mathbf{e}_{z0}$. Both nodes can move under applied load, however, it is possible to recompute the global deflections into relative values keeping one the rings fixed. In the present case the inner ring is chosen as the fixed reference one. The relative spatial position of the outer ring is justified by small displacements u_x, u_y and rotation angles γ_x, γ_y, gathered in the vector

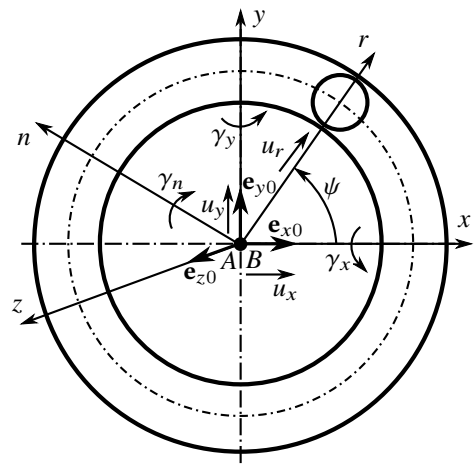

Figure 1. Bearing coordinate system, nodal displacements and forces.

$$\mathbf{y}_{rel} = \begin{bmatrix} u_x & u_y & 0 & \gamma_x & \gamma_y & 0 \end{bmatrix}^T, \tag{1}$$

which is related to the externally applied force vector

$$\mathbf{F} = \begin{bmatrix} F_x & F_y & 0 & M_x & M_y & 0 \end{bmatrix}^T. \tag{2}$$

The proposed model is incapable to carry axial load, thus the deflection u_z is not taken into account. Axial rotation γ_z is also absent due to bearing mechanics. The corresponding force vector components are nullified.

Let us introduce a local coordinate system r, n, z for each roller, such that axis r is aligned in the radial direction, axis z is inherited from the bearing node A and axis $n = r \times z$. Displacement vector (1) is written in the roller local coordinates system as

$$\mathbf{y}_{local} = \begin{bmatrix} v & \vartheta \end{bmatrix}^T = \mathbf{S}\mathbf{y}_{rel}, \tag{3}$$

where the rotation matrix

$$\mathbf{S} = \begin{bmatrix} \cos\psi & \sin\psi & 0 & 0 & 0 & 0 \\ 0 & 0 & 0 & -\sin\psi & \cos\psi & 0 \end{bmatrix} \tag{4}$$

was introduced. For statics analysis the position of the j-th roller is constant and defined as $\psi = j\theta$ with $\theta = \dfrac{2\pi}{N}$, where N is the number of rollers. In transient dynamics problems angle ψ varies according to the rotation phase of the outer ring relatively to the inner one, thus an arbitrary roller periodically enters and leaves the contact zone.

The outer ring cross-section at a particular rolling element is loaded by the force vector

$$\mathbf{P}_{local} = \begin{bmatrix} P_r & M_n \end{bmatrix}^T \tag{5}$$

and the bearing equilibrium can thus be written as

$$\mathbf{F} + \sum_{j=1}^{N} \mathbf{S}_j^T \mathbf{P}_{local\,j} = \mathbf{0}. \tag{6}$$

The constructed set of equations is nonlinear and the iterative Newton–Raphson scheme is invoked to determine the unknown vector $\mathbf{y}_{rel}$ for a given force vector $\mathbf{F}$:

$$\sum_{j=1}^{N} \mathbf{S}_j^T \mathbf{K}_{local\,j} \mathbf{S}_j \Delta \mathbf{y}_{rel} = \mathbf{F} + \sum_{j=1}^{N} \mathbf{S}_j^T \mathbf{P}_{local\,j}, \tag{7}$$

where the local roller stiffness matrix $\mathbf{K}_{local}$ was introduced.

2.2 Deformation pattern of a bearing ring

For simplicity, let us describe the deformed state of the bearing inner ring, analogous considerations hold for the outer one as well. The ring can be treated as an initially curved rod under a set of radial forces, see Figure 2a. In general case, the applied set of forces is not self-equilibrated, thus to perform static analysis some external kinematic constraints has to be imposed. Since their a priori definition is hardly possible (keeping in mind the housing and the shaft flexibility), an approximated approach of the ring deformed shape definition is proposed herein.

A classical strength of materials solution states that in a circular rod subjected to K equally distributed identical radial forces the contribution of the bending strains will vanish in comparison to the tensile ones as K grows [4]. In most bearings, especially used in aviation jet industry, the distribution of radial forces varies relatively smooth and to a certain degree of accuracy the ring can be treated as a set of segments of finite length, each of which is subjected to a constant compressive load N and a bending moment M. The error introduced by this simplification is particularly low for bearings with negative internal clearance and the operating regime, which is a common situation for jet engines. The assumption is similar to replacing the general deformation scheme of the bearing semicircle depicted in Figure 2c with a pattern that does not reproduce deflections at points C and D, which are negligible in comparison to the vertical displacement at point G.

Consider a circular rod with the centerline radius R_m, the cross section area A and the section modulus I. Being subjected to radial external load Q_r its segment of length $l = \theta R_m$, shown in Figure 2b, exhibit radial deflection w and the corresponding axil strain can be computed as

$$\varepsilon = \frac{\Delta l}{l} = \frac{\theta(R_m - w) - \theta R_m}{\theta R_m} = -\frac{w}{R_m}. \tag{8}$$

Recalling the Hook's law for one dimensional case, *i.e.*, $\sigma = \varepsilon E$, the potential energy of this tensile deformation renders:

$$T = \int_V \frac{1}{2} E \varepsilon^2 \,\mathrm{d}V = \int_0^{\theta R_m} \frac{1}{2} E A \frac{w^2}{R_m^2} A \,\mathrm{d}s = \frac{1}{2} E A \theta \frac{w^2}{R_m}. \tag{9}$$

Besides tension phenomenon, the radial deflection w also alters the segment curvature radius that results in appearance

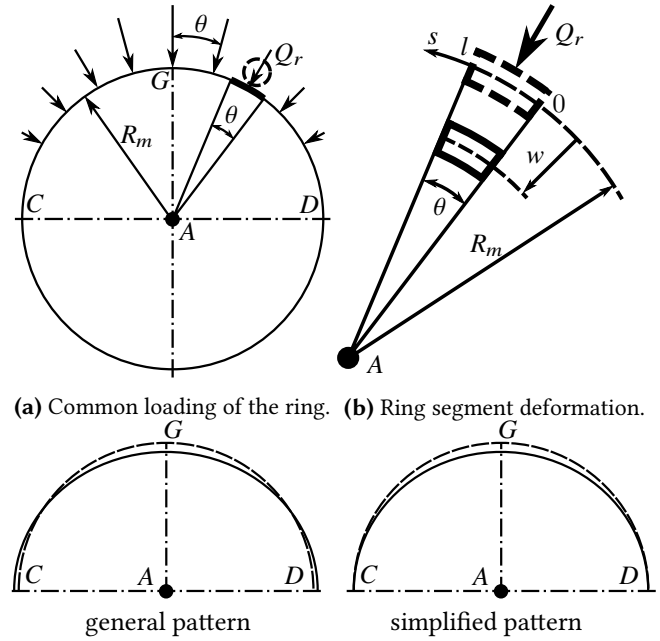

(a) Common loading of the ring. **(b)** Ring segment deformation.

(c) Ring deformation patterns.

Figure 2. Radial deformations of the bearing inner ring.

of pure bending. The corresponding deformation energy is [4]:

$$\begin{aligned} B &= \int_0^l \frac{M^2}{2EI} \,\mathrm{d}s = \int_0^{\theta R_m} \frac{1}{2} EI \left(\frac{1}{R_m - w} - \frac{1}{R_m} \right)^2 \mathrm{d}s \\ &= \frac{1}{2} EI\theta \frac{w^2}{R_m (R_m - w)^2}, \end{aligned} \tag{10}$$

where the following well known relation between the bending moment and the change of the curvature radius was applied:

$$\frac{1}{R_m - w} - \frac{1}{R_m} = \frac{M}{EI}. \tag{11}$$

Comparing expressions (9) and (10) we may observe that, indeed, $B << T$. This fact correlates with the initial hypothesis of the prevalence of tensile strains over bending ones.

2.3 Roller equilibrium

To obtain the roll load force vector $\mathbf{P}_{local}$ and the tangent stiffness matrix $\mathbf{K}_{local}$ let us describe the roller equilibrium for a given vector $\mathbf{y}_{local}$. Equilibrium of a roller in contact is determined by the following parameters:

- v_r - roller radial displacement,
- φ - roller rotation about axis n,
- w_i - radial deflection of the inner ring central line,
- w_e - radial deflection of the outer ring central line,

which are gathered in a single roller state vector

$$\mathbf{y}_{roll} = \begin{bmatrix} v_r & \varphi & w_i & w_e \end{bmatrix}^T. \tag{12}$$

We emphasize that the axial deflection of the roller remains prohibited. Such constraint is acceptable for small misalignment angles. Moreover, this axial degree of freedom is normally physically inadmissable due to presence of the cage. If necessary the misalignment angle can be completely neglected: in this case the roller degree of freedom φ and the corresponding outer ring rotation angles γ_x and γ_y are extracted from the model.

The essential bearing parameters required for its geometry definition are summarized in Figure 3a: R_p — pitch radius, R_i — radius of the inner ring raceway, R_e — radius of the outer ring raceway, R_b — roller radius (in case of profiled roller, radius at the central section), L — roller length, b — rings width (presently taken equal for both rings), R_h — outer radius of the housing, R_s — inner radius of the shaft (the last 3 parameters are needed only if rings flexibility is considered). The raceways radii can be computed from a given clearance value g (either positive or negative) via

$$R_i = R_p - R_b - \frac{g}{4} \quad \text{and} \quad R_e = R_p + R_b + \frac{g}{4}. \tag{13}$$

Figure 3b displays the deformed configuration of the bearing in a roller's cross section. The roller contact compressions between inner and outer rings at its central section are

$$\delta_i = -\frac{g}{4} - v_r - w_i \quad \text{and} \quad \delta_e = -\frac{g}{4} - v + v_r - w_e. \tag{14}$$

A roller may have a non-cylindrical profile. In this case its geometry is reproduced approximately by means of the slicing technique. The roller profile is discretized into a finite number of so-called cylindrical slices as shown in Figure 3a. For the k-th slice one should define its radius b_k, width h_k and distance s_k between its center and the roller central section. Slices do not need to have necessarily equal lengths and, for instance, for straight segments a single slice can be used to reproduce the original geometry. However, if misalignment degree of freedom φ is not neglected and needs to be treated, several slices are required even for a simple cylindrical profile. A roller with a single segment is not able to react on the misalignment appearance, since $s = 0$ and, therefore, its rotation stiffness is zero.

For each k-th slice Hertzian linear contact is implied, the distributed line load per unit length q_{ak} is then evaluated as [2]

$$q_{ak} = C_a \delta_{ak}^n, \tag{15}$$

where index $a = \{e, i\}$ highlights that the formula holds for both outer and inner ring. If k-th slice is in contact, $\delta_{ak} > 0$, otherwise $q_{ak} = 0$. The contact compressions at the k-th slice are computed from δ_a and φ:

$$\delta_{ik} = \delta_i - R_b + b_k - \varphi s_k, \tag{16a}$$

$$\delta_{ek} = \delta_e - R_b + b_k + (\varphi - \vartheta) s_k. \tag{16b}$$

The contact stiffness coefficient C_a depends on the material properties. If the same material with elasticity modulus E and Poisson ratio μ is used for manufacturing both rollers and rings, then the following relation holds:

$$C_a = \frac{\pi E L}{(1-\mu^2)\,(7.358L)^n}, \tag{17}$$

where for linear contact the exponent number $n = \frac{10}{9}$. We emphasize that within the proposed formulation radial ball bearings can be also treated. In this case the contact relation (15) is modified: the contact coefficients C_a and the exponent number n (for ball bearings $n = \frac{3}{2}$), and use of slicing technique is no longer required in this case.

Recalling (15), we may write the energy of the contact pair roller–ring as follows:

$$U_a = \frac{1}{n+1} \sum_{k=1}^{K} C_a \delta_{ak}^{n+1} h_k, \tag{18}$$

A roller is also subjected to the centrifugal inertia force, which is related with the kinetic energy as

$$V = \frac{1}{2} m \omega_c^2 \left(R_p + v_r\right)^2, \tag{19}$$

where m is the roller mass and ω_c is its rotation speed about the bearing axis. Therefore, referring to (9) and (10) the total energy functional of the roller clamped between two rings renders:

$$\Pi = U_e + T_e + B_e + U_i + T_i + B_i - V. \tag{20}$$

Minimization of Π delivers the roller equilibrium position and determines the unknown vector $\mathbf{y}_{roll}$. Components of the roller force vector and the tangent stiffness matrix are computed as the first and the second order derivative of the functional with respect to the components of $\mathbf{y}_{roll}$, *i.e.*,

$$P_{roll\,i} = -\frac{\partial \Pi}{\partial y_{roll\,i}}, \tag{21a}$$

$$K_{roll\,ij} = \frac{\partial^2 \Pi}{\partial y_{roll\,i} \partial y_{roll\,j}} \tag{21b}$$

or

$$\mathbf{P}_{roll} = -\frac{\partial \Pi}{\partial \mathbf{y}_{roll}} = \begin{bmatrix} Q_i - Q_e + F_c \\ M_i - M_e \\ Q_e - N_e \\ Q_i - N_i \end{bmatrix}, \tag{22}$$

where

$$Q_a = \sum_{k=1}^{K} C_a \delta_{ak}^n h_k, \tag{23a}$$

$$M_a = \sum_{k=1}^{K} C_a \delta_{ak}^n h_k s_k, \tag{23b}$$

$$N_a = \frac{E A_a \theta w_a}{R_{am}} + \frac{E I_a \theta w_a}{\left(R_{am} \pm w_a\right)^3}, \tag{23c}$$

$$F_c = m \omega_c^2 \left(R_p + v_r\right), \tag{23d}$$

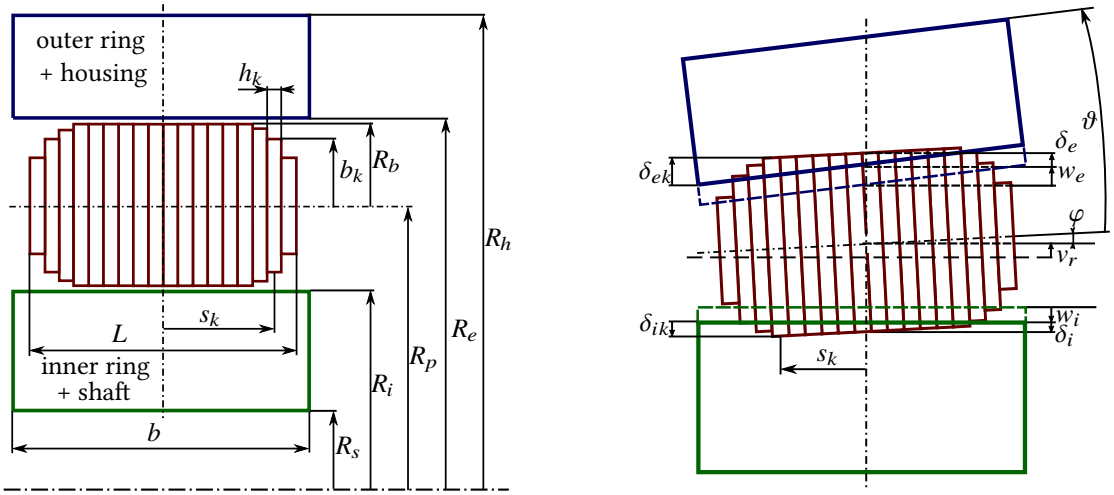

(a) Initial configuration. **(b)** Deformed configuration.

Figure 3. Initial and deformed configurations of the bearing roller and rings.

In (23c) "+" is used in case of the outer ring geometry ($a = e$) and "−" for the inner one ($a = i$). Rings geometric parameters A_a, I_a and R_{am} can be easily retrieved from Figure 3a. Similarly to (22) we may find analytical expression for the components of matrix $\mathbf{K}_{roll} = -\dfrac{\partial \mathbf{P}_{roll}}{\partial \mathbf{y}_{roll}}$, however, these are omitted here due to lack of space.

Roll equilibrium condition is obviously formulated as

$$\mathbf{P}_{roll} = \mathbf{o}. \tag{24}$$

The generated system of nonlinear equilibrium equations (24) can be resolved by means of the Newton–Raphson method. Note that for a given displacement vector of the outer ring the equilibrium position of each roller can be determined independently from the others, thus the iterative procedure is applied only to a small system of 4 equations with 4 unknowns. This positively influences performance and stability of the entire algorithm.

Once the roller equilibrium position is governed, the desirable stiffness matrix $\mathbf{K}_{full}$ introduced in (7) can be obtained. To this end we vary the energy functional (20) not only over the components of vector $\mathbf{y}_{roll}$, but also over the components of vector $\mathbf{y}_{local}$. This results in appearance of the following extended force vector and stiffness matrix:

$$\mathbf{P}_{full} = -\begin{bmatrix} \dfrac{\partial \Pi}{\partial \mathbf{y}_{roll}} \\ \dfrac{\partial \Pi}{\partial \mathbf{y}_{local}} \end{bmatrix} = \begin{bmatrix} \mathbf{P}_{roll} \\ \mathbf{P}_{ext} \end{bmatrix}, \tag{25}$$

$$\mathbf{K}_{full} = -\begin{bmatrix} \dfrac{\partial \mathbf{P}_{roll}}{\partial \mathbf{y}_{roll}} & \dfrac{\partial \mathbf{P}_{roll}}{\partial \mathbf{y}_{local}} \\ \dfrac{\partial \mathbf{P}_{ext}}{\partial \mathbf{y}_{roll}} & \dfrac{\partial \mathbf{P}_{ext}}{\partial \mathbf{y}_{local}} \end{bmatrix} = \begin{bmatrix} \mathbf{K}_{roll} & \mathbf{K}_{rr} \\ \mathbf{K}_{rr}^T & \mathbf{K}_{ext} \end{bmatrix}. \tag{26}$$

Notation in (26) reflects symmetry of the resultant matrix (this fact is easy to verify) that directly follows from existence of the functional. Submatrices from (26) are omitted herein due to cumbersomeness but can be easily derived.

Since the bearing element does not have any external degrees of freedom directly related to the rollers, we perform the static condensation procedure [20], taking the components of vector $\mathbf{y}_{local}$ as master degrees of freedom:

$$\mathbf{P}_{local} = \mathbf{P}_{ext} - \mathbf{K}_{rr}^T \mathbf{K}_{roll}^{-1} \mathbf{P}_{roll} = -\frac{\partial \Pi}{\partial \mathbf{y}_{local}} = \begin{bmatrix} Q_e \\ M_e \end{bmatrix}, \tag{27}$$

$$\mathbf{K}_{local} = \mathbf{K}_{ext} - \mathbf{K}_{rr}^T \mathbf{K}_{roll}^{-1} \mathbf{K}_{rr}. \tag{28}$$

When simplifying (27), we also imply that at the roller equilibrium position identity (24) holds.

2.4 Extension to multibody dynamics

The obtained expressions are valid for the situation when the inner ring if fixed and the outer exhibits small displacements and rotations. Consider nodes A and B of the bearing are allowed to have arbitrarily large deflections $\mathbf{u}$ and rotations $\boldsymbol{\theta}$ — the latter is the Euler vector [19]. The element state is then described by means of vector

$$\mathbf{y} = \begin{bmatrix} \mathbf{u}_A \\ \boldsymbol{\theta}_A \\ \mathbf{u}_B \\ \boldsymbol{\theta}_B \end{bmatrix}. \tag{29}$$

The Euler vector is related to the rotation tensor

$$\mathbf{Q} = \mathbf{I} + h_1(\theta)\,\boldsymbol{\Theta} + h_2(\theta)\,\boldsymbol{\Theta}^2, \tag{30}$$

where $\mathbf{I}$ — identity tensor, $\boldsymbol{\Theta} = \operatorname{skew}(\boldsymbol{\theta})$ — skew-symmetric tensor of vector $\boldsymbol{\theta}$ and scalar $\theta = \|\boldsymbol{\theta}\|$. Functions

$$h_1(\theta) = \frac{\sin\theta}{\theta} \quad \text{and} \quad h_2(\theta) = \frac{1}{2}\left(\frac{\sin\theta/2}{\theta/2}\right)^2 \tag{31}$$

were also introduced in (30).

The relative displacement of the outer ring in the coordinate system attached to node A can be evaluated as:

$$\boldsymbol{\xi} = \begin{bmatrix} u_x & u_y & u_z \end{bmatrix}^T = \mathbf{Q}_A^T \mathbf{u}_{BA} = \mathbf{Q}_A^T (\mathbf{u}_B - \mathbf{u}_A), \tag{32}$$

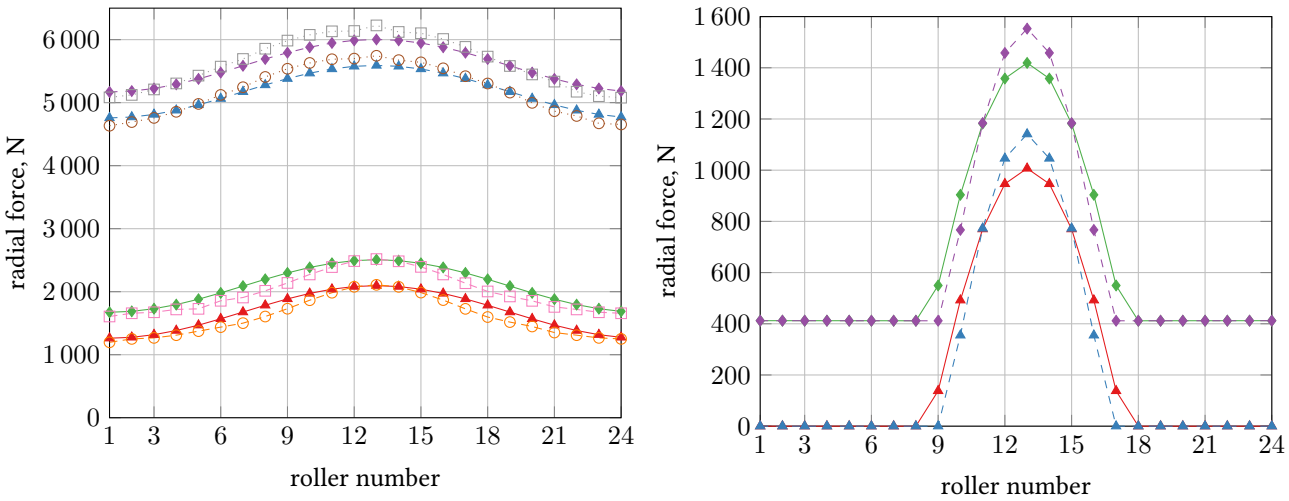

(a) negative clearance $g = -40\ \mu$m.

(b) positive clearance $g = 10\ \mu$m.

Q_i flexible rings	Q_i rigid rings	— proposed model
Q_e flexible rings	Q_e rigid rings	— proposed model
Q_i flexible rings	Q_i rigid rings	— NX Nastran
Q_e flexible rings	Q_e rigid rings	— NX Nastran

Figure 4. Distribution of bearing internal radial for different values of clearance.

whose variation after some vectorial math renders

$$\delta\boldsymbol{\xi} = \delta\left(\mathbf{Q}_A^T\mathbf{u}_{BA}\right) = \mathbf{X}\boldsymbol{\Gamma}_A^T\delta\boldsymbol{\theta}_A + \mathbf{Q}_A^T\delta\mathbf{u}_B - \mathbf{Q}_A^T\delta\mathbf{u}_A, \quad (33)$$

where $\mathbf{X} = \text{skew}\,(\boldsymbol{\xi})$, and also the well-known tangent tensor [12] appears:

$$\boldsymbol{\Gamma} = \mathbf{I} + h_2(\theta)\boldsymbol{\Theta} + h_3(\theta)\boldsymbol{\Theta}^2, \quad h_3\,(\theta) = \frac{1 - h_1(\theta)}{\theta^2}. \quad (34)$$

When deriving the first term of (33) we used the following expression, valid for any constant vector $\mathbf{t}$:

$$\begin{aligned}\delta\mathbf{Q}^T\mathbf{t} &= -\mathbf{Q}^T\text{skew}\,(\boldsymbol{\Gamma}\delta\boldsymbol{\theta})\,\mathbf{t} = \mathbf{Q}^T\mathbf{t}\times(\boldsymbol{\Gamma}\delta\boldsymbol{\theta}) \\ &= \mathbf{Q}^T\mathbf{t}\times\left(\mathbf{Q}^T\boldsymbol{\Gamma}\delta\boldsymbol{\theta}\right) = \mathbf{T}'\boldsymbol{\Gamma}^T\delta\boldsymbol{\theta},\end{aligned} \quad (35)$$

where $\mathbf{t}' = \mathbf{Q}^T\mathbf{t}$, $\mathbf{T}' = \text{skew}\,(\mathbf{t}')$. The following property [19] was also applied:

$$\mathbf{Q}^T\boldsymbol{\Gamma} = \boldsymbol{\Gamma}^T. \quad (36)$$

Similarly to (32), the relative rotation of the inner ring in the coordinate system attached to node A can be determined as

$$\boldsymbol{\gamma} = \begin{bmatrix}\gamma_x & \gamma_y & \gamma_z\end{bmatrix}^T = \mathbf{Q}_A^T\left(\mathbf{e}_{zA}\times\mathbf{e}_{zB}\right), \quad (37)$$

where unitary axial vectors of each bearing node at the deformed configuration are given by

$$\mathbf{e}_{zA} = \mathbf{Q}_A\mathbf{e}_{z0} \quad \text{and} \quad \mathbf{e}_{zB} = \mathbf{Q}_B\mathbf{e}_{z0}. \quad (38)$$

The variation of (37) can be obtained with the aid of (35) as:

$$\begin{aligned}\delta\boldsymbol{\gamma} = \mathbf{G}\boldsymbol{\Gamma}_A^T\delta\boldsymbol{\theta}_A &+ \mathbf{Q}_A^T\mathbf{E}_{zB}\mathbf{E}_{zA}\boldsymbol{\Gamma}_A\delta\boldsymbol{\theta}_A \\ &- \mathbf{Q}_A^T\mathbf{E}_{zA}\mathbf{E}_{zB}\boldsymbol{\Gamma}_B\delta\boldsymbol{\theta}_B\end{aligned} \quad (39)$$

with $\mathbf{G} = \text{skew}\,(\boldsymbol{\gamma})$, $\mathbf{E}_{zA} = \text{skew}\,(\mathbf{e}_{zA})$, $\mathbf{E}_{zB} = \text{skew}\,(\mathbf{e}_{zB})$. Recalling definitions (32) and (37) we can now rewrite (1) as

$$\mathbf{y}_{rel} = \begin{bmatrix}\boldsymbol{\xi} \\ \boldsymbol{\gamma}\end{bmatrix}, \quad (40)$$

whose variation with the aid of (33) and (39) can be formulated in a closed matrix form

$$\delta\mathbf{y}_{rel} = \mathbf{H}\delta\mathbf{y}, \quad (41)$$

where the following operator was defined:

$$\mathbf{H} = \begin{bmatrix}-\mathbf{Q}_A^T & \mathbf{O} & \mathbf{Q}_A^T & \mathbf{X}\boldsymbol{\Gamma}_A^T \\ \mathbf{O} & \mathbf{G}\boldsymbol{\Gamma}_A^T + \mathbf{Q}_A^T\mathbf{E}_{zB}\mathbf{E}_{zA}\boldsymbol{\Gamma}_A & \mathbf{O} & -\mathbf{Q}_A^T\mathbf{E}_{zA}\mathbf{E}_{zB}\boldsymbol{\Gamma}_B\end{bmatrix}. \quad (42)$$

Matrix $\mathbf{H}$, by fact, enhances the developed approach with capability to be used within the multibody dynamics formulation. When the bearing experiences large motions, operator (42) should be applied to the force vector and the stiffness matrix of the element:

$$\begin{aligned}\mathbf{P}_{tang} &= \mathbf{H}^T\sum_{j=1}^{N}\mathbf{S}_j^T\mathbf{P}_{local\,j}, \\ \mathbf{K}_{tang} &= \mathbf{H}^T\sum_{j=1}^{N}\mathbf{S}_j^T\mathbf{K}_{local\,j}\mathbf{S}_j\mathbf{H}.\end{aligned} \quad (43)$$

3. NUMERICAL EXAMPLE

3.1 Static analysis and comparison with FEM

Consider the radial bearing with 24 cylindrical rollers with dimensions $R_p = 75$ mm, $R_b = 6.5$ mm, $L = 16$ mm, $R_s =$

54 mm, $R_h = 97$ mm, $b = 30$ mm. Radial load $F_x = 5000$ N, the inner ring rotates with speed $\omega_{\text{rel}} = 12000$ rpm. Material elasticity modulus $E = 2 \cdot 10^{11}$ MPa, Poisson ratio $\mu = 0.3$ and density $\rho = 7850$ kg/m^3.

At first we analyze the bearing with negative clearance $g = -40$ μm[1]. If the bearing rings are treated as rigid, the obtained values of contact radial forces turn out to be 2.5 higher than for the case when structural deformations are permitted, as presented in Figure 4a. In case of minimal positive clearance $g = 10$ μm the influence of rings flexibility on the forces distribution is less crucial and can be neglected — that is, indeed, commonly done in practice (see Figure 4b). Figure 5 plots dependence of difference between the maximum radial load on the outer ring for the two situations when structural deformations are permitted and not, depending on clearance value g, *i.e.*, $\Delta Q_{e\max} = Q_{e\max}^{\text{rigid}} - Q_{e\max}^{\text{flexible}}$. The graph confirms the previously made statement that the rings flexibility plays more important role when the bearing operates with considerable negative clearance. If the clearance is nearly zero, the maximum radial force for two solutions is practically equal. Note that for large positive clearances the contribution of structural deformations in the bearing again becomes apparent, however not as significant as for the negative clearance of the same magnitude.

The obtained distribution of the radial forces for $g = -40$ μm was verified by FEM analysis performed with NX Nastran[2]. To this end a 3D model from Figure 6 was used. Surface traction $q_x(\varphi) = q_0 b \cos\varphi$ was distributed along the lower part of the inner ring raceway such, that $F_x = \int_{-\frac{\pi}{2}}^{\frac{\pi}{2}} q_0 b \cos\varphi \, \mathrm{d}\varphi$. Kinematic boundary conditions of the outer ring are difficult to determine, so the latter is attached from both ends to long thin cylinders with length 235 mm. The opposite sides of cylinders are clamped. In order to vanish the cylinders contribution to rigidity of the assembly, their elasticity modulus is set $E' = 0,01E$. The FEM model of the bearing with rigid rings is a lot simpler. In this case we fix the external surface of the outer ring and apply load F_x pointwisely at the inner ring central node, which is connected to the inner raceway surface with rigid elements. For each roller we also impose two constraints $u_z = 0$ at the central end face points to prevent their axial displacements.

According to Figure 4a, our model provides results which agree well those of NX Nastran for both rigid and flexible rings situations. The computation time for complete 3D model is quite substantial: it takes 45 minutes to perform static analysis of the model with structural rings deformations and 15 minutes for the configuration with rigid bearing rings. The proposed model is significantly faster and on the same hardware generates output in 2 and 1.5 seconds, respectively.

[1]To guarantee optimum bearing life, its internal clearance should remain as low as possible or slightly negative at operating mode. Due to design errors this requirement may be violated that seriously compromises bearing durability.

[2]FEM model of the bearing with positive clearance (for both flexible and rigid rings cases) was not built in NX Nastran within the present work due to its substantive complexity. Discussion of various aspects of such finite element problem itself can become a topic of a separate article.

3.2 Application to multibody dynamics

To demonstrate the applicability of the proposed approach for multibody dynamics problems the model from Figure 7a was analyzed. This assembly was designed in one of our research projects during the development of a 3D model of a planetary gearbox. The inner and outer rings of the bearing, whose parameters are given in Section 3.1, are located at nodes A and B, respively. The outer ring is connected to the basement C via the spatial rigid link element [9] of length $l = 1$ m, which uses Lagrange multipliers technique for imposition of kinematic constraints. All degrees of freedom of node C, except the axial rotation u_{rz}, are prohibited. The pointwise mass with $m_B = 2$ kg is located at node A. The basement node C rotates at an axial speed $\omega_C = 50$ rds ≈ 477 rpm. This value is specially chosen to provide the resultant centrifugal load, acting onto the mass at node A, identical to the value of the statically applied radial force from the first test, *i.e.*, $F = m_B l \omega_C^2 = 5000$ N. Independent rotation is also defined at node A. Its value $\omega_A = 12000 + \omega_C = 12477$ rpm is adjusted such that the relative rotation speed of the inner ring would coincide with ω_{rel} used in the aforementioned statics test. The internal negative clearance $g = -40$ μm is again introduced in the bearing and the rings structural deformations are permitted. Both rotations ω_A and ω_C are not applied instantly, but were set linearly increasing as shown in Figure 7b. To advance the solution the implicit Newmark integration scheme [8] is invoked.

Under these circumstances the obtained radial forces in the bearing are expected to agree with the ones obtained previously for the statics test. Indeed, the generated distributions of Q_e and Q_i totally coincide with plot from Figure 4a. Evolution of the radial forces acting on an arbitrary roller is plotted in Figure 7c. It is apparent that peaks in curves Q_e and Q_i perfectly correlate with maximum and minimum values of the respective quantities from Figure 4a.

3.3 Bearing misalignment

To access the model performance in the case of misalignment, the bearing 3.1 with negative clearance is loaded additionally with constant moment $M_y = 13.7$ Nm. The roller was discretized with 10 identical slices, the same mesh density along the roller length was used in NX Nastran to build contact regions with underlying solid elements. The applied moment does not change the distribution of the radial forces in the bearings (as expected), but rather influences the distribution of the contact pressure along the roller. Such behaviour was also confirmed by the FEM model, where a pair of forces with $\|F_z\| = 100$ N was applied at points G and H to reproduce the moment load. Figure 8 depicts distribution of the contact pressure along the most loaded roller number 13. The results are in good agreement with the FEM simulation. Note that NX Nastran computes contact forces at the grid nodes, while our approach provides values at the center of each slice — this fact justifies presence of significant drops in contact forces at the roller end faces. Regardless of these defects the resultant contact forces for both solutions are very close, see Figure 4a.

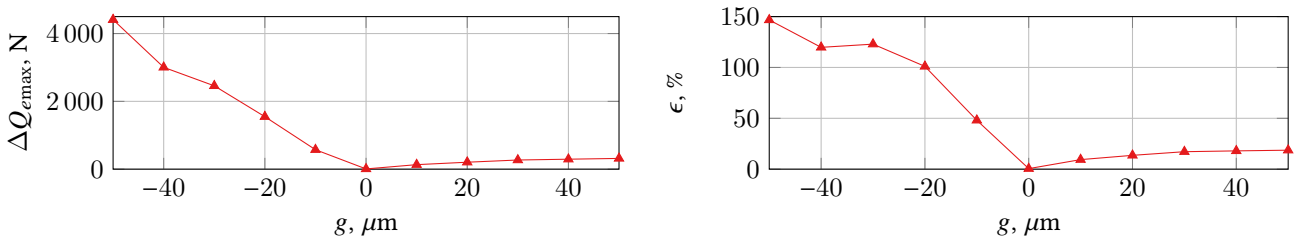

(a) Absolute error $\Delta Q_{e\max} = Q_{e\max}^{\text{rigid}} - Q_{e\max}^{\text{flexible}}$.

(b) Relative error $\epsilon = \dfrac{\Delta Q_{e\max}}{Q_{e\max}^{\text{flexible}}} \cdot 100\%$.

Figure 5. Contribution of accounted bearing rings flexibility on the maximum radial forces for different values of clearance.

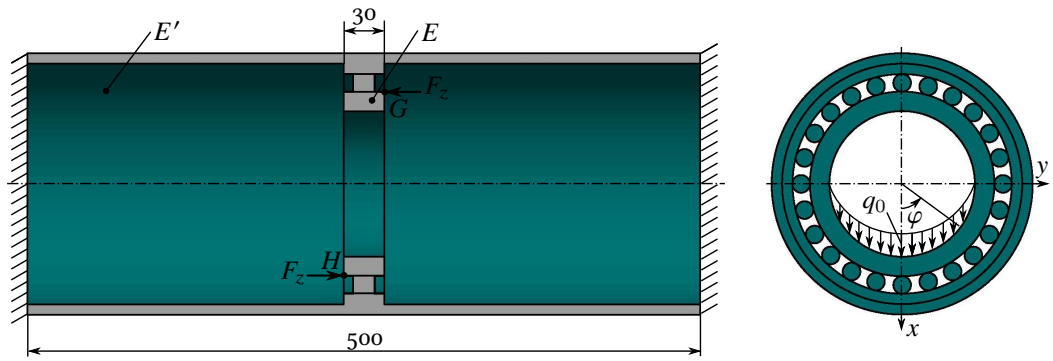

Figure 6. Model of the bearing with flexible rings in NX Nastran.

4. CONCLUSION

A model of radial bearing that accounts for structural deformations of its rings was presented. Numerical experiments disclosed that their contribution is particularly important for those situations when a negative clearance appears at the operating mode, while for regimes with positive clearance this behaviour can be neglected. The proposed mathematical model can be used with both spherical and cylindrical rolling elements. When dealing with the latter, the profiled geometry can be approximately reproduced by means of slicing technique. The equilibrium position of each rolling element is determined with a set of 4 variables: radial displacement and in-plane rotation of a roller and radial deflections of raceways of each of the two rings. Roller inertia properties are also considered. The model can be implemented in a 2-nodes finite element with 12 degrees of freedom and can be integrated practically into any FEM code.

Relative simplicity, high performance and robustness are the most apparent advantages of the proposed formulation. The obtained kinematic relations reliably detect entrance of a roller into the contact zone and its leaving. The internal iterative process that determines the roller equilibrium normally converges in 3–4 iterations. The fact that for each roller the Newton–Raphson process is launched independently positively impacts the overall performance of the model.

The model currently prohibits axial load to be applied. Addition of flanges and friction into the roller equilibrium along with introduction of axial degree of freedom for the rolling element could alleviate this issue. This enhancement will allow one to analyze radial-thrust bearing including those with tapered rollers. It is also necessary to capture more complex deformation patterns of the rings, especially for configurations when bending factor becomes essential relatively to the tensile strains. In this case determination of equilibrium for each rolling element can no longer be made independently and the bearing should be handled as a complete assembly of the two rings and the rollers with all internal degrees of freedom influencing each other.

REFERENCES

[1] S. Aihara. “A New Running Torque Formula for Tapered Roller Bearings Under Axial Load”. In: *Journal of Tribology* 109.3 (July 1987), pp. 471–477.

[2] S. Andréason. “Load distribution in a taper roller bearing arrangement considering misalignment”. In: *Tribology* 6.3 (1973), pp. 84–92.

[3] H. Aramaki, Y. Shoda, Y. Morishita, and T. Sawamoto. “The Performance of Ball Bearings With Silicon Nitride Ceramic Balls in High Speed Spindles for Machine Tools”. In: *Journal of Tribology* 110.4 (Oct. 1988), pp. 693–698.

[4] R. Budynas, W. Young, and A. Sadegh. *Roark’s Formulas for Stress and Strain, 8th Edition.* McGraw-Hill Education, 2011.

[5] G. Cavallaro, D. Nelias, and F. Bon. “Analysis of High–Speed Intershaft Cylindrical Roller Bearing with Flexible Rings”. In: *Tribology Transactions* 48.2 (2005), pp. 154–164.

[6] W. Cheng. “Experimental and Numerical Study of Multibody Contact System with Roller Bearing–Part II: Semi–Finite Element Analysis and Optimal Design

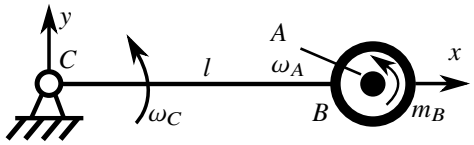

(a) Problem statement.

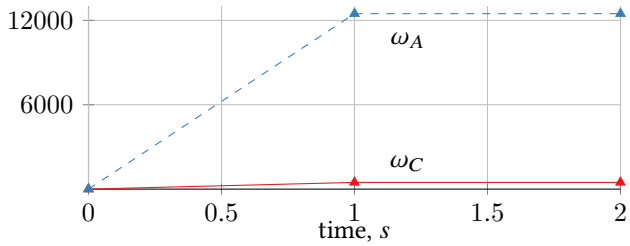

(b) Evolution of rotation speeds ω_C and ω_A.

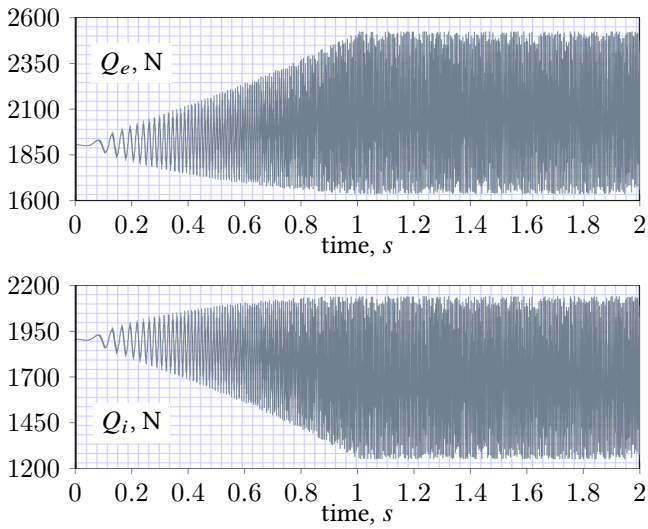

(c) Evolution of radial forces acting on a certain roller.

Figure 7. Transient analysis of the bearing with flexible rings and negative clearance $g = -40$ μm rotating about the fixed basement.

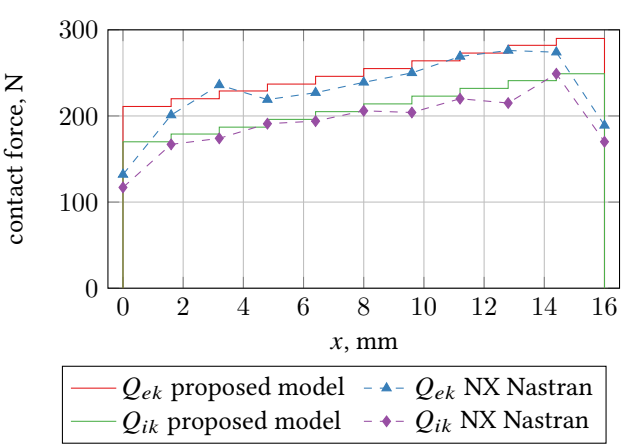

Figure 8. Distribution of contact forces along the bearing roller in the case of misalignment, $g = -40$ μm.

of Housing". In: *Tribology Transactions* 39.1 (1996), pp. 166–172.

[7] E. G. Filetti and J. H. Rumbarger. "A General Method for Predicting the Influence of Structural Support Upon Rolling Element Bearing Performance". In: *Journal of Lubrication Technology* 92.1 (Jan. 1970), pp. 121–127.

[8] B. Gavrea, D. Negrut, and F. A. Potra. *The Newmark Integration Method for Simulation of Multibody Systems: Analytical Considerations.* 2005.

[9] M. Géradin and A. Cardona. *Flexible multibody dynamics: a finite element approach.* Chichester, England: John Wiley, 2001.

[10] P. K. Gupta. *Advanced Dynamics of Rolling Elements.* 1st ed. Springer-Verlag New York, 1984.

[11] T. A. Harris. *Rolling Bearing Analysis, 4th Edition.* 4th ed. 2000.

[12] V. Ivannikov. "A geometrically exact Kirchhoff–Love shell model: theoretical aspects and a unified approach for interpolative and non-interpolative approximations". PhD thesis. Instituto Superior Técnico, Technical University of Lisbon, 2014.

[13] A. B. Jones and T. A. Harris. "Analysis of a Rolling-Element Idler Gear Bearing Having a Deformable Outer-Race Structure". In: *Journal of Basic Engineering* 85.2 (June 1963), pp. 273–278.

[14] A. Leblanc, D. Nelias, and C. Defaye. "Nonlinear dynamic analysis of cylindrical roller bearing with flexible rings". In: *Journal of Sound and Vibration* 325.1–2 (2009), pp. 145–160.

[15] J. Y. Liu. "Analysis of Tapered Roller Bearings Considering High Speed and Combined Loading". In: *Journal of Lubrication Technology* 98.4 (Oct. 1976), pp. 564–572.

[16] J. M. de Mul, J. M. Vree, and D. A. Maas. "Equilibrium and Associated Load Distribution in Ball and Roller Bearings Loaded in Five Degrees of Freedom While Neglecting Friction–Part I: General Theory and Application to Ball Bearings". In: *Journal of Tribology* 111.1 (1989), pp. 142–148.

[17] J. M. de Mul, J. M. Vree, and D. A. Maas. "Equilibrium and Associated Load Distribution in Ball and Roller Bearings Loaded in Five Degrees of Freedom While Neglecting Friction–Part II: Application to Roller Bearings and Experimental Verification". In: *Journal of Tribology* 111.1 (1989), pp. 149–154.

[18] A. Palmgren. *Ball and roller bearing engineering.* 1959.

[19] C. Tiago. "Meshless methods: Extending the linear formulation and its generalization to geometrically exact structural analysis". PhD thesis. Instituto Superior Técnico, Technical University of Lisbon, 2007.

[20] O. C. Zienkiewicz, R. L. Taylor, and J. Z. Zhu. *Finite Element Method: Its Basis and Fundamentals.* sixth. Vol. 1. Elsevier Butterworth–Heinemann, 2005.